Crustal conditions favoring convective downward migration of fractures in deep hydrothermal systems

Sæunn Halldorsdottir[1], Inga Berre[2], Eirik Keilegavlen[1], and Gudni Axelsson[3]

[1]University of Bergen
[2]University of Bergen, Norway
[3]Iceland Geosurvey

August 4, 2023

Abstract

Cooling magma plutons and intrusions are the heat sources for hydrothermal systems in volcanic settings. To explain system longevity and observed heat transfer at rates higher than those explained by pure conduction, the concept of fluid convection in fractures that deepen because of thermal rock contraction has been proposed as a heat-source mechanism. While recent numerical studies have supported this half a century old hypothesis, understanding of the various regimes where convective downward migration of fractures can be an effective mechanism for heat transfer is lacking. Using a numerical model for fluid flow and fracture propagation in thermo-poroelastic media, we investigate scenarios for which convective downward migration of fractures may occur. Our results support convective downward migration of fractures as a possible mechanism for development of hydrothermal systems, both for settings within active zones of volcanism and spreading and, under favorable conditions, in older crust away from such zones.

Hosted file

968212_0_art_file_11166391_rxfh6l.docx available at https://authorea.com/users/638393/articles/654215-crustal-conditions-favoring-convective-downward-migration-of-fractures-in-deep-hydrothermal-systems

Crustal conditions favoring convective downward migration of fractures in deep hydrothermal systems

Sæunn Halldórsdóttir[1], Inga Berre[1], Eirik Keilegavlen[1], and Gudni Axelsson[2]

[1]University of Bergen, Center for Modeling of Subsurface Dynamics, Department of Mathematics, University of Bergen, Allégaten 41, 5007 Bergen.

[2]ÍSOR, Icelandic GeoSurvey, Urdarhvarf 8, 203 Kópavogur.

Corresponding author: Sæunn Halldorsdottir (saeunn.halldorsdottir@uib.no)

Key Points:

- Numerical modeling supports convective downward migration of fractures as a source mechanism for hydrothermal systems
- Fluid flow, fracture opening and propagation in a thermo-poroelastic rock mass are simulated in different geological settings in the crust
- Crustal stresses are key to understanding whether a hydrothermal system can evolve in regions away from active zones of volcanism

Abstract

Cooling magma plutons and intrusions are the heat sources for hydrothermal systems in volcanic settings. To explain system longevity and observed heat transfer at rates higher than those explained by pure conduction, the concept of fluid convection in fractures that deepen because of thermal rock contraction has been proposed as a heat-source mechanism. While recent numerical studies have supported this half a century old hypothesis, understanding of the various regimes where convective downward migration of fractures can be an effective mechanism for heat transfer is lacking. Using a numerical model for fluid flow and fracture propagation in thermo-poroelastic media, we investigate scenarios for which convective downward migration of fractures may occur. Our results support convective downward migration of fractures as a possible mechanism for development of hydrothermal systems, both for settings within active zones of volcanism and spreading and, under favorable conditions, in older crust away from such zones.

Plain Language Summary

Geothermal energy is transferred through and stored in the rock and fluids of the earth's crust. If temperature increases sufficiently with depth and the crust provides sufficient pathways for water to flow through, colder water sinks and percolates downward, gets heated at depth and then rises due to its lower density at higher temperature. This creates a hydrothermal circulation system that transports heat from the deep crust to shallower depths from where it can be produced. Wells drilled into these systems produce hot water and/or steam for direct heat utilization or electricity production. To understand the renewability of hydrothermal systems, we need to understand how heat is transferred deep in the crust. A hypothesis has been proposed, suggesting that fractures, propagating downwards because of contraction of the water-cooled surrounding rock, are central to maintaining the heat transfer from the deep crust. Based on settings in Iceland, we show how the fluid flow and propagation of fractures can be important for development of hydrothermal systems, using computer simulations, both in active regions of volcanism and, under favorable conditions, also in older crust away from such regions. The latter results are important for the identification of hidden geothermal systems.

1 Introduction

Hydrothermal fluid circulation within the earth's crust is driven by the combination of sufficient heating from below and permeability for fluids to flow (Lapwood, 1948). It is an important mechanism of mass and heat transfer in the crust and is seen as the explanation of anomalous temperature profiles with depth that are not consistent with heat transfer by conduction alone (Elder, 1965; Pálmason, 1967). While the concept was originally developed considering porous rocks, it was later expanded to include rocks with secondary permeability in the form of fractures, dikes and other structural features providing the main fluid conduits (Bodvarsson & Lowell, 1972). For hydrothermal systems, Bodvarsson and Lowell (1972) suggested how contraction induced by buoyancy-driven convective cooling would lead to tensile fracture opening and consequently strongly affect permeability at depth. A conceptual model of fractures migrating downwards due to convective cooling was described further by Lister (1974) and Bodvarsson (1982), including also analytical estimates of propagation speeds based on simplifying assumptions. Bodvarsson (1982) was the first to name the process "convective downward migration of fractures" (CDM) and specifically considered its role in transferring heat from cooling magma bodies to hydrothermal system over the lifespan of the hydrothermal activity. As the magma cools, a layer of gradually thickening solidified rock develops, providing an insulation between the heat source and the hydrothermal system. If this layer is impermeable, and the intrusive intensity of the magma is low, heat transfer from the magma to the hydrothermal system will decrease with time, which is inconsistent with the high heat output of such systems over long time scales (Bodvarsson, 1982; Björnsson et al., 1982). For hydrothermal systems in Iceland, Bodvarsson (1982) argued that the intrusive intensity would be low, and, hence, hypothesized CDM to be an important mechanism for heat transfer.

Bodvarsson, (1982; 1983) and Axelsson (1985) also suggested that CDM could be effective as a source mechanism in systems with elevated heat flux but away from central magmatic heat sources, and may account for some of the long-lasting low-enthalpy hydrothermal activity in the Icelandic crust. For such settings, they both proposed that the onset of the process would depend on local stress conditions. Such settings are not only limited to Iceland but can also be found in other areas (Jolie et al., 2021; Limberger et al., 2018). A better understanding of the settings controlling the highly coupled processes governing CDM may therefore also shed light on the existence of hydrothermal systems in other parts of the world.

While a comprehensive understanding of the geological settings where CDM can occur is still lacking, two recent numerical modeling studies support the hypothesis. Patterson & Driesner, (2021) present a model of large-scale natural convection in a downward propagating fracture zone (of dimensions: H=3km, L=8km, W=1m) in a thermo-elastic medium, considering what we in the present context will denote a low geothermal gradient of 55°C/km. They investigate the effect of thermoelastic rock stresses and fracture fluid pressure on fracture-zone transmissivity by use of a Barton-Bandis relationship between fracture transmissivity and effective normal stress (Bandis et al., 1983; Barton et al., 1985). Expanding on the conceptual model by Lister (1974) and Axelsson (1985), Stefansson et al., (2021b) present a fully coupled numerical approach for fracture propagation and deformation that allow for multiple fractures in a thermo-poroelastic medium. The effect of thermo-poroelastic stresses on fracture transmissivity is incorporated through a fracture contact mechanics model. In the work of Stefansson et al. (2021b), the downward migration of fractures due to convective cooling is considered for a test case with a set of smaller fractures (H=200m, L=200m, W=2mm) at the bottom of a geothermal system. The study applied parameters which are representative for a geothermal system in a geological setting with a high geothermal gradient of 150°C/km.

In this paper we use numerical modeling to investigate CDM as a source mechanism for hydrothermal activity. We consider both young crust in active zones of volcanism and spreading as well as older crust away from such zones. The numerical approach builds on the methodology by Stefansson et al. (2021b), accounting for flow and fracture propagation in thermo-poroelastic media. This enables us to study effects of the stress regime and thermal gradients, as well as effects of important rock parameters such as the permeability in the medium surrounding the fractures. The results by Stefansson et al. (2021b) indicate that CDM can be a plausible source mechanism in systems away from central heat sources if the thermal gradient is sufficiently high. Furthermore, it is clear that local stress setting (e.g. in spreading systems) can be favorable for CDM. This leads to the following hypotheses:

1. No central magmatic heat sources are needed for CDM, a high geothermal gradient is sufficient to maintain the process.

2. With lower geothermal gradients, crustal stress conditions in a range of geological settings are still favorable for CDM as a mechanism for heat transfer.

Using simulation models, we test these hypotheses with different thermal gradients, and show how, for lower thermal gradients found away from volcanic belts, local stress settings are a dominating factor for the onset of CDM.

As basis for the simulations, geological conditions found in Iceland are chosen. Iceland is famous for its hydrothermal systems providing its nation with both electricity and space heating through the utilization of geothermal fluids. Zones of spreading and volcanism cut through the center of the country along the Mid-Atlantic Ridge, explaining the elevated heat content in its crust. The volcanic belts rockmainly consist of very long fracture-zones dominated by spreading and injection of extremely long dikes at depth. Several central volcano complexes are interspersed in the zone, but these take up a very small part of the total area of the zone. For the study of CDM two regional settings are chosen, (1) within the spreading zone but away from any central volcanoes and (2) away from the spreading zone. Those two settings provide scenarios with elevated heat flux, that we in the present context will denote by a high geothermal gradient on one hand and low geothermal gradient on the other hand. As discussed in section 2, similar settings can be found in other regions of the world.

2 Geological settings for CDM

Compared to normal conditions on the earth's surface, the heat flux through hydrothermally active areas is elevated. In systems located within volcanically active areas one might assume that intense magma intrusion frequency and resulting conduction, could at least partly sustain these systems (Björnsson et al., 1982; Gunnarsson et al., 2010); however, this is an unlikely case for most systems (Bodvarsson, 1954; Hochstein, 1995; Weir, 2001). We will look at the effect of thermal stress changes, induced by cooling at depth by buoyancy driven convection, and how this process can lead to enhanced permeability and heat transfer by convection in propagating fractures. The process of fracture propagation at depth allows for thermal fluid being in direct contact with hot formation deep within the systems (White, 1968; Björnsson et al., 1982; Bjornsson & Stefansson, 1987). The process evolves over time to give fluid access to new parts of the rock, which can be related to the lifetime and the intensity of hydrothermal activity. Hence, CDM should be considered as a possible source mechanism of hydrothermal activity.

We study a model of vertical fractures in the roots of geothermal systems, first proposed by Lister (1974) and Bodvarsson (1982). Convection of geothermal fluid in the fractures cools down the surrounding rock, causing horizontal tensile stresses in the rock, which lead to (1) the rock to contract and (2) the fractures to propagate downward. By this self-sustained process, the convection of thermal fluid extends downward constantly reaching fresh hot rock, enhancing the heat flux to the geothermal system above. The process, combined with heat conduction, could sustain the hydrothermal systems in accordance with observed heat output.

2.1 Extension deformation that favors vertical permeability

Areas of elevated heat flow and heat content that favor the development of hydrothermal systems are located at divergent plate boundaries, where the spreading of the lithosphere leads to ascending magma and intrusion into the crust. Regional extension tectonics create both regional and local structures that furthermore affect permeability. Some examples of divergent plate boundaries include the Mid-Atlantic Ridge, Red Sea Rift, Baikal Rift Zone, East African Rift (Great Rift Valley), East Pacific Rise, Gakkel Ridge, Galapagos Rise, Explorer Ridge, Juan de Fuca Ridge, Pacific-Antarctic Ridge, and West Antarctic Rift System. Many hydrothermal systems are located in those settings, for example in Iceland (mid-Atlantic Ridge), Eritrea, Djibouti, Ethiopia, Uganda, Kenya, Tanzania and Malawi (western and eastern branches of the East Africa Rift) (Hochstein, 2005). Hydrothermal vents along the seabed are known to form along divergent mid-ocean ridges, such as the East Pacific Rise and the Mid-Atlantic Ridge (Petersen et al., 2018).

Divergent plate boundaries are examples of extension-controlled tectonics. Extension deformation that can enhance vertical permeability can also be found in locations away from convergent or transform plate boundaries, such as in back-arc basins (Lau Basin in the East Pacific), in continental extension zones (Rio Grande Rift Zone, East-African Rift Zone, Western Turkey (Bozkurt & Mittwede, 2005), and in releasing bends along strike-slip faults and in zones of thickened crust (gravitational spreading). Known areas of hydrothermal activity associated with continental rifting are, for example, located in the Great Basin in Western USA, the countries in the western and eastern branches of the East African Rift, in west Turkey and in Cyprus (Bettison-Varga et al., 1992; Murat Özler, 2000). Areas of hydrothermal activity associated with back-arc activity are e.g. located in the Taupo Volcanic Zone New Zealand (Kissling & Weir, 2005), and the Okinawa Trough Japan (Halbach et al., 1989; Yang et al., 2020).

Extension deformation due to reginal tectonics alone can act to enhance vertical permeability and therefore give rise to the circulation of fluids at intermediate depths in the crust. This, however, does not explain increased hydrothermal activity in tectonically less active areas. Pálmason, (1981) speculated on the effect of cooling of the lithosphere as it moves away from the rift axis and suggests that thermal stresses consequently induce enhanced vertical permeability for geothermal fluids at depths on the flanks of the active rifting. Hence, we consider the effects of fluid circulation in existing fractures and how increased thermal stress may cause fracture propagation, thus increasing vertical permeability. It is expected that both temperature settings in the crust and regional stresses influence the initiation and maintenance of CDM.

3 Mathematical and numerical modeling of CDM

We use a mathematical model based on a discrete fracture matrix representation. The medium is 3D, consisting of the rock matrix and embedded fractures modelled as 2D planes. The model describes energy transport and fluid flow in rock matrix and fractures, thermo-poroelastic deformation of the rock, and fracture deformation and propagation. We assume single phase fluid conditions with the reservoir rock fully saturated, and with local thermal equilibrium between the fluid and the solid. We impose a balance of momentum, mass and energy in the rock matrix and a balance of mass and energy in the fractures, along with kinematic constraints and constitutive laws for fracture deformation (Stefansson et al., 2021a; see also Barton, 1976). In the following, key components of the model are reviewed. A full description of the mathematical model, including coupling between variables in the rock matrix and the fracture (Jaffré et al., 2011; Martin et al., 2005; Stefansson et al., 2021b), is provided in the supplementary material of this paper.

Dimension reduction of the balance equations which is necessary to derive the flow of mass and energy in the fracture is detailed in Stefánsson et al. (2021a) and Keilegavlen et al. (2021a).

The aperture of a dimensionally reduced fracture is given by

$$a = a_0 + [\![\mathbf{u}]\!]_{\mathrm{n}}. \quad (1)$$

Here, a_0 is the residual hydraulic aperture in the undeformed state, and $[\![\mathbf{u}]\!]_{\mathrm{n}}$ the normal component of a displacement-jump over the fracture, defined as the difference in the displacement, $\mathbf{u}$, computed on the opposing fracture walls. The fracture aperture, a, will be affected by fluid pressure as well as thermo-poromechanical forces in the matrix. The flow in the fracture is described by Darcy's law with a cubic law for the permeability, giving a strongly non-linear relation between the aperture and the fluid flow.

We consider propagation due to tensile forces, modeled by the stress intensity factor (Stefansson et al., 2021b; se also Nejati et al., 2015),

$$SI_{\mathrm{I}} = \sqrt{\frac{2\pi}{R_d}}\left(\frac{\mu}{\kappa + 1}[\![\mathbf{u}]\!]_{\mathrm{n}}\right), \quad (2)$$

where R_d is the distance between the point where the displacement jump is evaluated and the fracture tip, μ is the shear modulus of the rock, and κ is the Kolosov constant for plain strain described as a function of the shear and the bulk moduli of the rock (see supplementary material). The fracture tip propagates when SI_{I} exceeds a critical value,

$$SI_{\mathrm{I}} \geq SI_{Icrit}, \quad (3)$$

which can be viewed as the rock toughness.

The mathematical model is implemented in the open-source simulation tool PorePy, which is tailored for representing complex multiphysics processes in fractured porous media (Keilegavlen et al., 2021a). The fractures are explicitly represented in the computational grid which allows for direct modelling of processes in the fracture and on the fracture walls. In the computational grid, pressure and temperature are represented in both rock matrix and fractures, the displacement is confined to the rock matrix and on the fracture walls, and contact tractions are represented on the fractures. Fracture propagation is represented by extending the fracture grid, with minimal adjustments needed to the rest of the computational model.

4 Simulations of CDM in different geological settings

Two regional settings are considered to investigate the process of CDM as a source mechanism for hydrothermal activity. They are both considered representative of temperature conditions in the crust of Iceland: (1) within the Icelandic active zone of volcanism and spreading and (2) in older crust away from the active zone of spreading. The first represents regions rich with geothermal resources while the second represents regions which are considered to include fewer geothermal systems (Axelsson, et al., 2005). The heat source is thermal energy within the earth's crust, accumulated over time by heat flow from the lithosphere and intrusive activity. The background thermal gradient is 100-150°C/km (Flóvenz & Saemundsson, 1993) in young crust within the rifting zone, and varies between 50° and 100°C/km in older crust further away from the divergent ridge axis. These settings are distinct from known volcano complexes with associated high-enthalpy hydrothermal activity and heat sources of magmatic origin.

The depth at which fissures are assumed to be open varies between those regions: Close to the divergent axis, within the active zone, we assume fissures to be open down to 2 km depth, whereas away from the axis, in colder crust, we assume fissures to be open down to 1 km depth. Isothermal temperature with depth profiles from geothermal fields in Iceland strengthen this assumption (Arnórsson et al., 2008; Axelsson, et al., 2000; Björnsson et al., 2000; Xianghui, 2012). We assume that the depth of open fissures reflect the depth of the geothermal systems in the initial state of the simulations. Since we are investigating the longevity of the systems and the CDM as a key mechanism to maintain the systems, we consider the opening and propagation of fractures beyond those depths.

4.1 Simulation domain and setup

For the numerical investigation of different geological settings, we choose a three-dimensional domain, a cube with side-lengths of 400 m. At the top of the domain, five evenly spaced vertical planar fractures are located along the x-axis, each spanning 200 m in length and depth. The formation depth and thermal gradients are set in accordance with the two regional settings: For the two regional settings considered, the geothermal gradient is set accordingly to (1) 130 °C/km and (2) 80 °C/km, representing temperature conditions within and away from the active zone, respectively. The top of the simulation domain is located at (1) a depth of 2000 m and (2) a depth of 1000 m, respectively, thus the temperature at the top of the domain is 260 °C and 80 °C, respectively, for the two different cases. We denote settings corresponding to (1) as high-temperature (HT) regimes and settings corresponding to (2) as low-temperature (LT) regimes, respectively.

The background stress field is aligned with respect to the fractures, with vertical stress (S_V) equal to the weight of the overburden, the maximum horizontal stress (S_H) in direction of the fractures (along the y-axis), and the minimum horizontal stress (S_h) perpendicular to the fractures (x-axis). This background stress implies that fractures are favorably oriented for opening and propagation. Figure 1 (leftmost) shows the initial geometrical setup of the domain and the fractures.

The background stress is defined such that

$$S_h = \sigma_{xx} = b_1\sigma_{zz},\ S_H = \sigma_{yy} = b_2\sigma_{zz},\ S_V = \sigma_{zz} = \rho_S g z, \tag{4}$$

where ρ_S is the bulk density of the overburden, g is the acceleration of gravity, z is the depth and b_1 and b_2 are positive constants. Four background stress regimes (A-D) are defined (Table 1) for b_1 = {0.4, 0.6} and for b_2 = {0.8, 1.2}. The choice of the background stress, which corresponds to either a strike-slip or a normal fault regime, is based on stress settings observed in Iceland (Ziegler et al., 2016), away from the central volcanism and therefore also away from the complex stress conditions associated with volcanic activity.

Motivated by the assumption of a low rock porosity of 5%, the bulk density of the overburden is set equal to that of the rock. The matrix permeability is assumed to be 10 μD and the residual aperture to be 2 mm. Those values are in the lower range of what is suggested by measurements in active systems (Keilegavlen et al., 2021b; Massiot et al., 2017; Sigurdsson et al., 2000). The linear thermal expansion of the rock is chosen according to the temperature conditions at the two different settings, with the thermal expansion coefficient for the high temperature case set five times larger than for the second case, see Table 1 (Yin et al., 2021). The thermal expansion coefficient of water and water viscosity is chosen according to the overall temperature, while other parameters are constant, across the two different regional settings (1 and 2) shown in Table 1.

Table 1: Background-stress for regimes A-B and parameters for regional settings 1&2, defining conditions for the eight different cases modelled. Parameters that are identical for both settings are highlighted in gray.

Stress regime	**A**	**B**	**C**	**D**
σ_{xx}	0.6 σ_{zz}	0.4 σ_{zz}	0.4 σ_{zz}	0.6 σ_{zz}
σ_{yy}	1.2	1.2 σ_{zz}	0.8 σ_{zz}	0.8 σ_{zz}
σ_{zz}	$\rho_S g\, z$	$\rho_S g\, z$	$\rho_S g\, z$	$\rho_S g\, z$
Regional setting		**1**	**2**	
Parameter	***Symbol***	***Values***	***Values***	***Units***
Depth @top of domain	z_0	2000	1000	M
Temp. gradient with depth	dT/dz	0.13	0.08	$\mathrm{°C/m}$
Temperature @top of domain	T_0	260	80	°C
Dynamic viscosity	η	1.1×10^{-4}	3.5×10^{-4}	Pa s
Fluid volumetric thermal expansion	β_f	4×10^{-4}	2×10^{-4}	$\mathrm{°C^{-1}}$
Solid linear thermal expansion	β_s	5×10^{-5}	1×10^{-5}	$\mathrm{°C^{-1}}$
Bulk modulus of the fluid	B_f	2.5×10^{9}	2.5×10^{9}	Pa
Bulk modulus of the rock	B_S	2.2×10^{10}	2.2×10^{10}	Pa
Biot coefficient	α	0.8	0.8	–
Reference fluid density	$\rho_{0,f}$	1×10^{3}	1×10^{3}	$\mathrm{kg\ m^{-3}}$
Reference solid density	$\rho_{0,s}$	2.7×10^{3}	2.7×10^{3}	$\mathrm{kg\ m^{-3}}$
Fluid specific heat	c_f	4.2×10^{3}	4.2×10^{3}	$\mathrm{J\ kg^{-1}\ °C^{-1}}$
Solid specific heat	c_s	7.9×10^{2}	7.9×10^{2}	$\mathrm{J\ kg^{-1}\ °^{-1}}$
Fluid thermal conductivity	κ_f	0.6	0.6	$\mathrm{W\ m^{-1}\ °C^{-1}}$
Solid thermal conductivity	κ_s	2.0	2.0	$\mathrm{W\ m^{-1}\ °C^{-1}}$
Fluid compressibility	c	4×10^{-10}	4×10^{-10}	$\mathrm{Pa^{-1}}$
Shear modulus of the rock	μ	2×10^{10}	2×10^{10}	Pa
Matrix porosity	ϕ	0.05	0.05	–
Matrix permeability	k	1×10^{-17}	1×10^{-17}	$\mathrm{m^2}$
Residual aperture	a_0	2.0×10^{-3}	2.0×10^{-3}	m
Friction coefficient	F	0.8	0.8	–
Dilation angle	ψ	3.0	3.0	°
Critical stress intensity factor	SI_{Icrit}	5×10^{5}	5×10^{5}	Pa

Dirichlet boundary conditions are chosen for the temperature and pressure. This means that temperature gradient and hydrostatic pressure are fixed on the sides of the numerical domain. At the top of the domain the boundary conditions are imposed on both the rock matrix and the fractures. Neumann boundary conditions are chosen for the displacement by imposing the anisotropic tractions defined in Table 1, assuming zero displacement in the centre of the bottom boundary. Considering the onset of natural convection, these boundary conditions represent a conservative choice given the prescribed linear temperature profile on the vertical boundaries.

4.2 Results

In total, eight simulations were run, representing eight different geological settings, based on the two regional settings (1-2) and the four background stress regimes (A-D). For the HT regimes, onset of propagation occurs for all the four background stress conditions shown in Table 1. For the LT regimes, onset of propagation only occurs for cases B and C.

The modelled fracture evolution can be seen in Figure 1, that shows the modeled temperature in all five fractures: Before fracture propagation (left) and at the end of the simulation (center) for setting 2C (LT, normal stress), and at the end of the simulation for setting 1A (HT, strike-slip) (right). At the end of the simulation period the middle fracture has propagated 160m and 180m downward, respectively, in the LT and HT cases. The average speed of the migrating front is therefore 3.3 and 3.5 m/year for the two different cases.

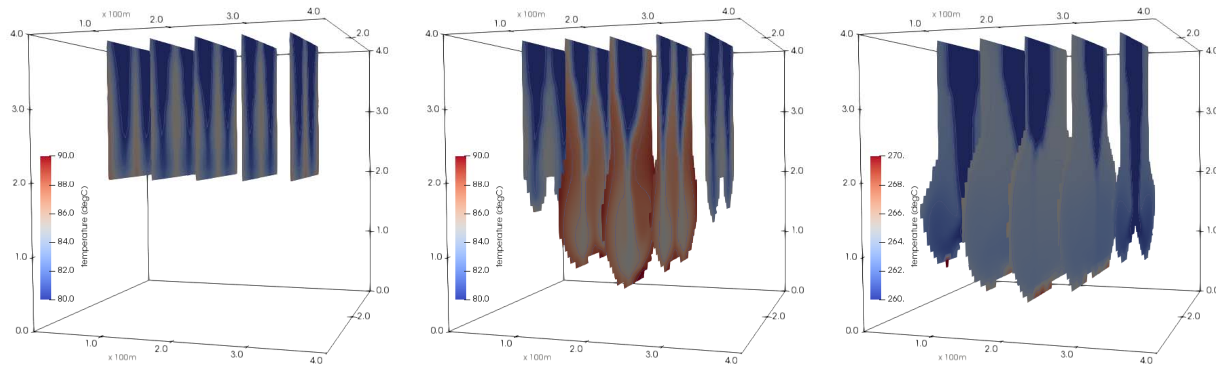

Figure 1: Temperature distribution in the five fractures: Left: Setting 2C (low temperature, normal stress) after 10 years simulation time (before onset of propagation), therefore, also showing the original geometry of the domain. Center: Setting 2C at the end of the simulation (60 yr.). Right: Setting 1A (high temperature, strike-slip stress) at the end of the simulation (60 yr.).

The onset of propagation and the propagation speed of the five fractures is shown in Figure 2 for the six simulations where propagation occurs. The onset of propagation in HT regimes (1A to 1D) is after 7-8 years, for the thermal expansion coefficient set according to the predicted thermal conditions at 2 km depth within the crust. However, with thermal expansion coefficient set according to the predicted thermal conditions at 1 km depth within the crust in the LT setting (2), there is no onset of propagation for stress regimes A and D, when the background minimum horizontal stress is 60% of the vertical stress. When the background minimum horizontal stress is 40% of the vertical stress (2B and 2C), the thermal stress imposed in the vicinity of the fracture is sufficient to overcome the background stress. The onset of propagation in those settings is after 12-13 years. Based on additional simulation studies, the transition to a regime of propagation is estimated to occur when the minimum horizontal stress is between 45% and 40% of the vertical stress.

In Figure 3 the Darcy velocity in the center fracture is shown for the low temperature case after 50 and 60 years. As the figure shows, fluid circulation in the fracture forms convection cells, however the flow pattern and number of cells change as the fracture propagates. This pattern is observed in both HT and LT cases and is due to changes in the fracture geometry as well as coupling to the surrounding rock matrix.

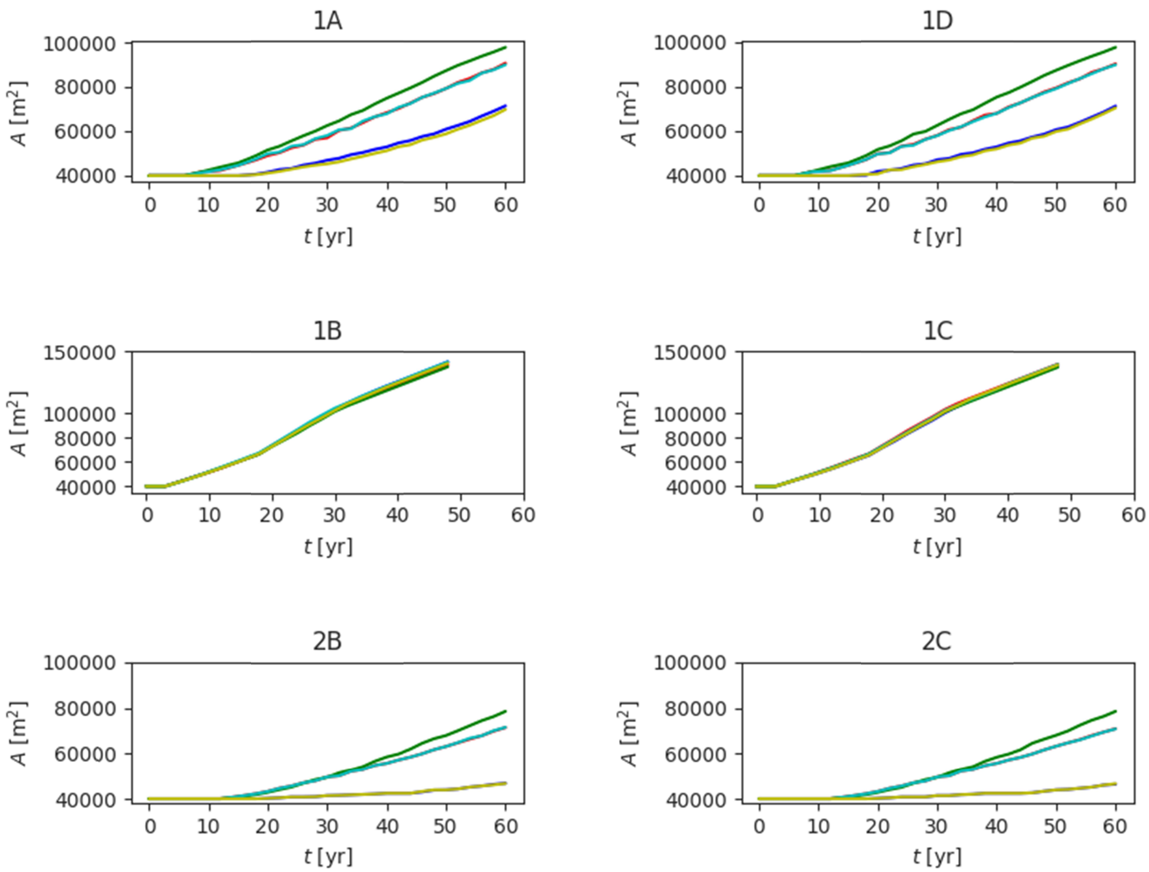

Figure 2: Propagation of the five fractures depicted as growth in surface area of each fracture. The high temperature regimes are presented in the upper two rows and the low temperature regimes in the bottom row. The left side involves a strike-slip background stress regime, and the right side a normal background stress regime.

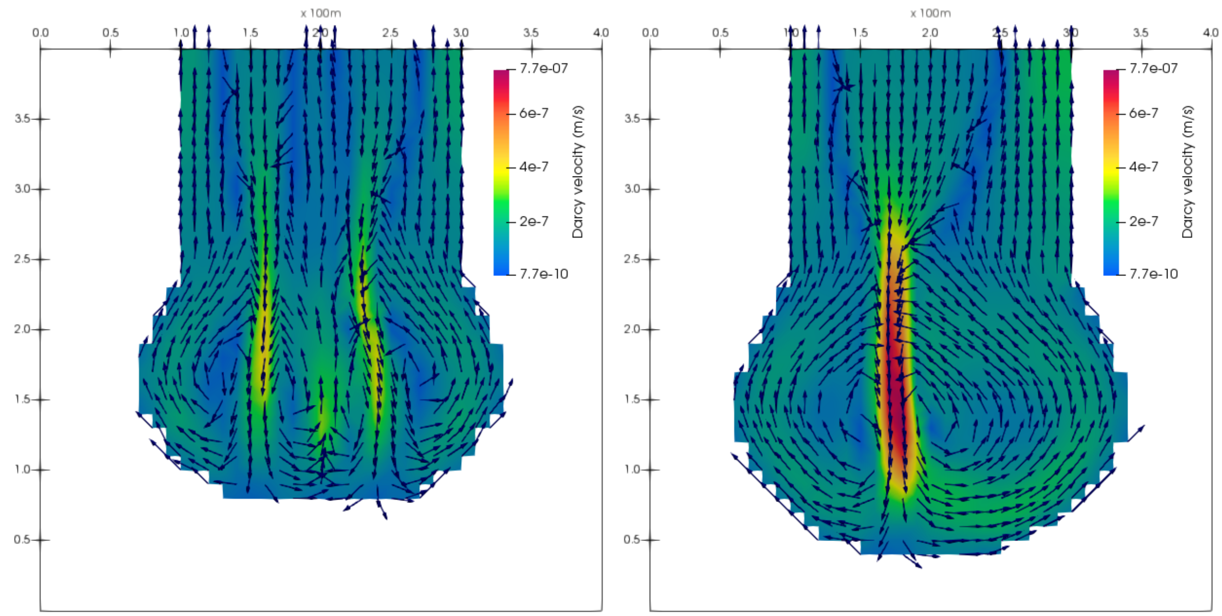

Figure 3: Darcy velocity in the center fracture in setting 2C (low temperature, normal stress), with the permeability related to the aperture by the relation $K_l = a^2/12$, after 50 and 60 years simulation time (left and right, respectively).

5 Conclusions

Our results contribute to ongoing discussion on (a) the convective downward migration of fractures (CDM) in the roots of geothermal systems, and (b) CDM's importance in explaining the origin and sustainability of hydrothermal activity. Many have contributed to the development of the mathematical model and description of the phenomenon; however, the complexity of the coupled processes of fluid flow, heat transfer and fracture and rock deformation, have put limitations on its understanding. Based on numerical simulations, we show that this process is plausible in different geological settings known to host hydrothermal systems.

The results of the numerical study show that the proposed CDM is highly relevant in understanding the nature of hydrothermal systems and the origin of hydrothermal activity. Notably, the study shows that CDM is possible in settings away from central heat sources, such as magma or cooling intrusion. As proposed by Bodvarsson (1982; 1983) and Axelsson (1985), a relatively low geothermal gradient is sufficient to initiate the process. This suggestion is supported by a resent numerical study (Patterson and Driesner, 2021). We have further shown that, in the absence of a high thermal gradient (e.g., in old crust away from active zones of volcanism and spreading), the local stress settings are important. The present numerical simulations show that CDM is possible in both strike-slip and normal stress regimes. In the case of lower thermal gradient, the stress perpendicular to the fracture must be low compared to the vertical stress—as already pointed out by previous studies, but now strengthened by results of the present numerical simulation. Therefore, our results indicate that crustal stresses are a clue as to whether a hydrothermal system can evolve in regions away from volcano-tectonic activity. In the search for hidden hydrothermal activity, this could be a key factor.

Acknowledgments

This project has received funding from the Norwegian Research Council, grant number 308733, and the VISTA program, The Norwegian Academy of Science and Letters and Equinor.

Open Research

The data and source code for the results presented herein is available at https://doi.org/10.5281/zenodo.8123952, and the results can be reproduced using version 1.4.2 of PorePy (Keilegavlen et al., 2021a).

References

Arnórsson, S., Axelsson, G., & Sæmundsson, K. (2008). Geothermal systems in Iceland. *Jökull, 58*(1), 269–302. doi.org/10.33799/jokull2008.58.269

Axelsson G. (1985). Hydrology and thermomechanics of liquid-dominated hydrothermal systems in Iceland, (Doctoral dissertation). Retrieved from ScholarsArchive@OSU. (https://ir.library.oregonstate.edu/concern/graduate_thesis_or_dissertations/ms35tc96f). Oregon State University.

Axelsson, G., Bjornsson, G., Egilson, T., Flovenz, O. G., Gautason, B., Hauksdottir, S., et al. (2005). Nature and Properties of Recently Discovered Hidden Low-Temperature Geothermal Reservoirs in Iceland. In *Proceedings of the World Geothermal Congress 2005: Antalya, Turkey, 24-29 April 2005*. Auckland, International Geothermal Association.

Axelsson, G., Flovenz, O. G., Hjartarson, A., Hauksdottir, S., Sverrisdottir, G., Arnason, F., et al. (2000). Thermal energy extraction by reinjection from the Laugaland geothermal system in N-Iceland. In *Proceedings of the World Geothermal Congress, 2000: Kyushu-Tohoku, Japan, May*

28-June 10, 2000. Tokyo; Auckland, Japanese Organizing Committee for WGC 2000; International Geothermal Association.

Bandis, S. C., Lumsden, A. C., & Barton, N. R. (1983). Fundamentals of rock joint deformation. *International Journal of Rock Mechanics and Mining Sciences & Geomechanics Abstracts, 20*(6), 249–268. doi.org/10.1016/0148-9062(83)90595-8

Barton, N. (1976). The shear strength of rock and rock joints. *International Journal of Rock Mechanics and Mining Sciences & Geomechanics Abstracts, 13*(9), 255–279. doi.org/10.1016/0148-9062(76)90003-6

Barton, N., Bandis, S., & Bakhtar, K. (1985). Strength, deformation and conductivity coupling of rock joints. *International Journal of Rock Mechanics and Mining Sciences & Geomechanics Abstracts, 22*(3), 121–140. doi.org/10.1016/0148-9062(85)93227-9

Bettison-Varga, L., Varga, R. J., & Schiffman, P. (1992). Relation between ore-forming hydrothermal systems and extensional deformation in the Solea graben spreading center, Troodos ophiolite, Cyprus. *Geology, 20*(11), 987–990. doi.org/10.1130/0091-7613(1992)020<0987:RBOFHS>2.3.CO;2

Björnsson, G., Thordarson, S., & Steingrímsson, B. (2000). Temperature distribution and conceptual reservoir model for geothermal fields in and around the city of Reykjavík, Iceland. In

Proceedings, Twenty-fifth Workshop on Geothermal Reservoir Engineering. (SGP-TR-165). Stanford CA, Stanford University.

Björnsson, H., Björnsson, S., & Sigurgeirsson, T. (1982). Penetration of water into hot rock boundaries of magma at Grímsvötn. *Nature,* 295. doi.org/10.1038/295580a0

Bjornsson, S., & Stefansson, V. (1987). Heat and Mass Transport in Geothermal Reservoirs. In J. Bear & M. Y. Corapcioglu (Eds.), *Advances in Transport Phenomena in Porous Media* (pp. 143–183). Springer Netherlands. doi.org/10.1007/978-94-009-3625-6_5

Bodvarsson, G. (1954). Terrestrial Heat Balance in Iceland. *J. Eng. Assoc., Iceland, 39*(6), 69–76.

Bodvarsson, G. (1982). Terrestrial Energy Currents and Transfer in Iceland. In G. Pálmason (Ed.), *Continental and Oceanic Rifts* (pp. 271–282). American Geophysical Union (AGU). doi.org/10.1029/GD008p0271

Bodvarsson, G. (1983). Temperature/flow statistics and thermomechanics of low-temperature geothermal systems in Iceland. *Journal of Volcanology and Geothermal Research, 19*(3), 255–280. doi.org/10.1016/0377-0273(83)90114-2

Bodvarsson, G., & Lowell, R. P. (1972). Ocean-floor heat flow and the circulation of interstitial waters. *Journal of Geophysical Research (1896-1977), 77*(23), 4472–4475. doi.org/10.1029/JB077i023p04472

Bozkurt, E., & Mittwede, S. K. (2005). Introduction: Evolution of continental extensional tectonics of western Turkey. *Geodinamica Acta, 18*(3–4), 153–165. doi.org/10.3166/ga.18.153-165

Elder, J. W. (1965). Physical Processes in Geothermal Areas. In W.H.K. Lee (Ed.), *Terrestrial Heat Flow* (Vol. 8, pp. 211–239). American Geophysical Union (AGU). doi.org/10.1029/GM008p0211

Flóvenz, Ó. G., & Saemundsson, K. (1993). Heat flow and geothermal processes in Iceland. *Tectonophysics, 225*(1), 123–138. doi.org/10.1016/0040-1951(93)90253-G

Gunnarsson, G., Arnaldsson, A., & Oddsdóttir, A. L. (2000). Model Simulations of the Geothermal Fields in the Hengill Area, South-Western Iceland. *Proceedings World Geothermal Congress 2010 Bali, Indonesia, 25-29 April 2010*. International Geothermal Association

Halbach, P., Nakamura. K., Wahsner, M., Lange, J., Sakai, H., Käselitz, L., et al. (1989), Probable modern analogue of Kuroko-type massive sulphide deposits in the Okinawa Trough back-arc basin. *Nature,* 338, 496–499. doi.org/10.1038/338496a0

Hochstein, M. P. (2005). Heat Transfer by Hydrothermal Systems in the East African Rifts. In *Proceedings of the World Geothermal Congress 2005: Antalya, Turkey, 24-29 April 2005*. Auckland, International Geothermal Association.

Hochstein, M. P. (1995). Crustal heat transfer in the Taupo Volcanic Zone (New Zealand): Comparison with other volcanic arcs and explanatory heat source models. *Journal of Volcanology and Geothermal Research, 68*(1), 117–151. doi.org/10.1016/0377-0273(95)00010-R

Jaffré, J., Mnejja, M., & Roberts, J. E. (2011). A discrete fracture model for two-phase flow with matrix-fracture interaction. *Procedia Computer Science, 4*, 967–973. doi.org/10.1016/j.procs.2011.04.102

Jolie, E., Scott, S., Faulds, J., Chambefort, I., Axelsson, G., Gutiérrez-Negrín, L. C., et al. (2021). Geological controls on geothermal resources for power generation. *Nature Reviews Earth & Environment,* 2, 324–339. doi.org/10.1038/s43017-021-00154-y

Keilegavlen, E., Berge, R., Fumagalli, A., Starnoni, M., Stefansson, I., Varela, J., & Berre, I. (2021). PorePy: An open-source software for simulation of multiphysics processes in fractured porous media. *Computational Geosciences, 25*(1), 243–265. doi.org/10.1007/s10596-020-10002-5

Keilegavlen, E., Duboeuf, L., Dichiarante, A. M., Halldórsdóttir, S., Stefansson, I., Naumann, M., et al. (2021). Hydro-mechanical simulation and analysis of induced seismicity for a hydraulic stimulation test at the Reykjanes geothermal field, Iceland. *Geothermics,* 97, 102223. doi.org/10.1016/j.geothermics.2021.102223

Kissling, W. M., & Weir, G. J. (2005). The spatial distribution of the geothermal fields in the Taupo Volcanic Zone, New Zealand. *Journal of Volcanology and Geothermal Research, 145*(1), 136–150. doi.org/10.1016/j.jvolgeores.2005.01.006

Lapwood, E. R. (1948). Convection of a fluid in a porous medium. *Mathematical Proceedings of the Cambridge Philosophical Society*, 44(4), 508–521. doi.org/10.1017/S030500410002452X

Limberger, J., Boxem, T., Pluymaekers, M., Bruhn, D., Manzella, A., Calcagno, P., et al. (2018). Geothermal energy in deep aquifers: A global assessment of the resource base for direct heat utilization. *Renewable and Sustainable Energy Reviews,* 82, 961–975. doi.org/10.1016/j.rser.2017.09.084

Lister, C. R. B. (1974). On the Penetration of Water into Hot Rock. *Geophysical Journal International, 39*(3), 465–509. doi.org/10.1111/j.1365-246X.1974.tb05468.x

Martin, V., Jaffré, J., & Roberts, J. E. (2005). Modeling Fractures and Barriers as Interfaces for Flow in Porous Media. *SIAM Journal on Scientific Computing, 26*(5), 1667–1691. doi.org/10.1137/S1064827503429363

Massiot, C., Townend, J., Nicol, A., & McNamara, D. D. (2017). Statistical methods of fracture characterization using acoustic borehole televiewer log interpretation. *Journal of Geophysical Research: Solid Earth, 122*(8), 6836–6852. doi.org/10.1002/2017JB014115

Murat Özler, H. (2000). Hydrogeology and geochemistry in the Curuksu (Denizli) hydrothermal field, western Turkey. *Environmental Geology, 39*(10), 1169–1180. doi.org/10.1007/s002540000139

Nejati, M., Paluszny, A., & Zimmerman, R. W. (2015). On the use of quarter-point tetrahedral finite elements in linear elastic fracture mechanics. Engineering Fracture Mechanics, 144, 194–221. doi.org/10.1016/j.engfracmech.2015.06.055

Pálmason, G. (1967). On heat flow in Iceland in relation to the Mid-Atlantic Ridge. In S. Björnsson (Ed.), *Iceland and mid-ocean ridges*. Reykjavík Iceland, Vis. Isl. (Societas Scientiarum Islandica).

Pálmason, G. (1981). Crustal rifting, and related thermo-mechanical processes in the lithosphere beneath Iceland. *Geologische Rundschau, 70*(1), 244–260. doi.org/10.1007/BF01764325

Patterson, J. W., & Driesner, T. (2021), Elastic and Thermoelastic Effects on Thermal Water Convection in Fracture Zones. *Journal of Geophysical Research: Solid Earth, 126*(2), e2020JB020940. doi.org/10.1029/2020JB020940

Petersen, S., Lehrmann, B., & Murton, B. J. (2018), Modern Seafloor Hydrothermal Systems: *New Perspectives on Ancient Ore-Forming Processes. Elements, 14*(5), 307–312. doi.org/10.2138/gselements.14.5.307

Sigurdsson, Ó., Gudmundsson, Á., Fridleifsson, G. Ó., Franzson, H., Gudlaugsson, S. T., & Stefánsson, V. (2000). Database on igneous rock properties in icelandic geothermal systems. Status and unexpected results. In *Proceedings of the World Geothermal Congress, 2000: Kyushu-Tohoku, Japan, May 28-June 10, 2000*. Tokyo; Auckland, Japanese Organizing Committee for WGC 2000; International Geothermal Association.

Stefansson, I., Berre, I., & Keilegavlen, E. (2021). A fully coupled numerical model of thermo-hydro-mechanical processes and fracture contact mechanics in porous media. *Computer Methods in Applied Mechanics and Engineering, 386*, 114122. doi.org/10.1016/j.cma.2021.114122

Stefansson, I., Keilegavlen, E., Halldórsdóttir, S., & Berre, I. (2021). Numerical Modelling of Convection-Driven Cooling, Deformation and Fracturing of Thermo-Poroelastic Media. *Transport in Porous Media, 140*(1), 371–394. doi.org/10.1007/s11242-021-01676-1

Weir, G. (2001), Heat Output from Spreading and Rifting Models of the Taupo Volcanic Zone, New Zealand. *Journal of Applied Mathematics and Decision Sciences, 5*(2), 105–118. doi.org/10.1207/S15327612JAMD0502_5

White, D. E. (1968). Hydrology, activity, and heat flow of the Steamboat Springs thermal system, Washoe County, Nevada. (Report No. 458C; Professional Paper). USGS Publications Warehouse. doi.org/10.3133/pp458C

Xianghui, W. (2012). Reservoir assessment of the Ósabotnar low-temperature geothermal field, SW-Iceland. (UNU-GTP Reports 2012 No. 38). Retrieved from GRÓ GTP (https://www.grocentre.is/gtp/moya/page/msc-theses-and-fellow-projects-2012). Reykjavík, UNU Geothermal Training Program.

Yang, B., Liu, J., Shi, X., Zhang, H., Wang, X., Wu, Y., & Fang, X. (2020). Mineralogy and sulfur isotope characteristics of metalliferous sediments from the Tangyin hydrothermal field in the southern Okinawa Trough. *Ore Geology Reviews,* 120, 103464. doi.org/10.1016/j.oregeorev.2020.103464

Yin, W., Feng, Z., & Zhao, Y. (2021). Effect of Grain Size on the Mechanical Behaviour of Granite Under High Temperature and Triaxial Stresses. *Rock Mechanics and Rock Engineering, 54*(2), 745–758. doi.org/10.1007/s00603-020-02303-z

Ziegler, M., Rajabi, M., Heidbach, O., Hersir, G. P., Ágústsson, K., Árnadóttir, S., & Zang, A. (2016). The stress pattern of Iceland. *Tectonophysics, 674*, 101–113. doi.org/10.1016/j.tecto.2016.02.008

Geophysical Research Letters

Supporting Information for

Crustal conditions favoring convective downward migration of fractures in deep hydrothermal systems

Sæunn Halldórsdóttir[1], Inga Berre[1], Eirik Keilegavlen[1], and Gudni Axelsson [2]

[1]University of Bergen, Center for Modeling of Subsurface Dynamics, Department of Mathematics, University of Bergen, Allégaten 41, 5007 Bergen.

[2]ÍSOR, Icelandic GeoSurvey, Urdarhvarf 8, 203 Kópavogur.

Contents of this file

Introduction

This document provides the governing equations that underlies the simulation model used for the paper 'Crustal conditions favoring convective downward migration of fractures in deep hydrothermal systems', referred to below as 'the paper'. It is divided into the following subsections:

- Thermo-poroelasticity, energy and mass balance in the rock matrix
- Fracture deformation and energy and mass balance in the fracture
- Tensile stress and fracture propagation
- Notes on the numerical implementation

Text S1.

For the modelling of hydrothermal reservoirs, we use a mathematical model based on a discrete fracture matrix method, that describes energy transport and fluid flow in a fractured deformable porous medium. The medium is 3D, consisting of rock matrix and embedded fractures modelled as 2D planes. Single phase fluid is assumed, fully saturating the reservoir rock. Furthermore, local thermal equilibrium between the fluid and the solid is assumed. Effective coefficients for the fluid saturated rock matrix are estimated based on the fluid and rock coefficients and the porosity, ϕ, according to:

$$(\text{coeff.})_{\mathrm{e}} = \phi(\text{coeff.})_{\mathrm{f}} + (1-\phi)(\text{coeff.})_{\mathrm{s}}. \tag{1}$$

We impose a balance of momentum, mass and energy in the rock matrix and balance of mass and energy in the fractures. The conservation equations described in this section are complemented by appropriate boundary conditions on the domain boundary (both matrix and fracture) described in section 4 of the paper.

Thermo-poroelasticity, energy and mass balance in the rock matrix

For quasi-static conditions, the linear momentum balance equation for an elementary volume in the rock matrix is given as

$$\nabla \cdot \boldsymbol{\sigma} = -\mathbf{F}, \tag{2}$$

with **F** being the body force per unit volume, and the total stress **σ** being composed of thermal, hydraulic and mechanical (THM) terms. By assuming linearity and using the convention that tensile stresses are positive, the stress-strain relationship for thermo-poroelasticity, resulting from perturbations from an initial temperature T_0 can be written

$$\boldsymbol{\sigma} = \mathrm{D}\!:\left(\nabla\mathbf{u} + \nabla\mathbf{u}^{\mathrm{T}}\right)/2 - \alpha p\mathbf{I} - \beta_s B_s (T - T_0)\mathbf{I}, \tag{3}$$

where D is the drained stiffness matrix and the strain is related to the displacement vector of the rock, $\mathbf{u}$ by the symmetric gradient $\left(\nabla\mathbf{u} + \nabla\mathbf{u}^{\mathrm{T}}\right)/2$. Furthermore, α is the Biot coefficient, p is fluid the pressure, $\mathbf{I}$ is the identity matrix, β_s and B_s are the volumetric thermal expansion and the bulk modulus of the rock, respectively, and ':' denotes the double dot product. Finally, we assume an isotropic medium and use $\mathrm{D}\!:\left(\nabla\mathbf{u} + \nabla\mathbf{u}^{\mathrm{T}}\right)/2 = \lambda\,\mathrm{tr}(\nabla\mathbf{u}) + \mu\left(\nabla\mathbf{u} + \nabla\mathbf{u}^{\mathrm{T}}\right)$, where μ is the shear modulus of the rock, and λ the Lame coefficient. Using that $\lambda = B_s - 2\mu/3$, the momentum balance for thermo-poroelasticity becomes

$$\nabla \cdot \left[(B_s - \tfrac{2}{3}\mu)\,\mathrm{tr}(\nabla\mathbf{u})\mathbf{I} + \mu\left(\nabla\mathbf{u} + \nabla\mathbf{u}^{\mathrm{T}}\right) - \beta_s B_s (T - T_0)\mathbf{I} - \alpha p\mathbf{I}\right] = -\mathbf{F}. \tag{4}$$

The fluid is assumed to be pure water and is modelled as slightly compressible

$$\rho_f = \rho_0 \exp\left[\frac{1}{B_f}(p - p_0) - \beta_f (T - T_0)\right], \tag{5}$$

with β_f and B_f, the thermal expansion and the bulk modulus of the fluid, respectively.

The Darcy velocity of the fluid within the rock is given by

$$\mathbf{v} = -\frac{k}{\eta}\left(\nabla p - \rho_f \mathbf{g}\right). \tag{6}$$

Here k is the matrix permeability, η is the fluid dynamic viscosity, and **g** the gravity vector.

To complete the thermo-poromechanics descriptions of the reservoir matrix balance of mass and energy is imposed. The mass balance equation is given by

$$\left(\frac{\phi}{B_f} + \frac{\alpha - \phi}{B_s}\right)\frac{\partial p}{\partial \mathrm{t}} + \alpha\frac{\partial}{\partial \mathrm{t}}(\nabla \cdot \mathbf{u}) - \beta_e \frac{\partial T}{\partial \mathrm{t}} + \nabla \cdot \mathbf{v} = \mathrm{Q_p}, \tag{7}$$

while the energy balance is governed by

$$\rho_e c_e \frac{\partial T}{\partial \mathrm{t}} + \beta_s K_s T_0 \frac{\partial}{\partial \mathrm{t}} (\nabla \cdot \mathbf{u}) + \nabla \cdot \left[\rho_f c_f T \mathbf{v} - \kappa_e \nabla T\right] = \mathrm{Q_T}. \tag{8}$$

Heat and volumetric sources and sinks are represented by $\mathrm{Q_T}$ and $\mathrm{Q_p}$ respectively. The effective thermal expansion and conductivity tensors of the rock matrix are given by β_e and κ_e, respectively, the effective density and specific heat by ρ_e and c_e, respectively, and the specific heat of the fluid is given by c_f. Based on the assumption that the fluid is all in liquid phase, a low enthalpy description is used, that is, the internal energy of the fluid takes the same form as the internal energy of the rock. This results in a simplification in the energy equation, with, $\rho_e c_e$, being the effective heat capacity of the rock matrix.

The primary variables in the rock matrix are the temperature T, the pressure p and the displacement $\mathbf{u}$.

Fracture deformation and energy and mass balance in the fracture

Dimension reduction for the mass and energy equations is necessary to derive the flow of mass and energy in the fluid-filled fractures. The dimension reduction is detailed in Stefansson et al., (2021a) and Keilegavlen et al. (2021a). For the mechanical forces on the fracture, we consider balance between the fracture contact traction force, $\boldsymbol{\lambda}_F$, and fracture fluid pressure, p_F, and the higher-dimensional THM traction on the opposing fracture walls (fracture-matrix interfaces):

$$\begin{aligned} \boldsymbol{\lambda}_F - p_F \mathbf{I} \cdot \boldsymbol{n}_M^+ &= \quad \boldsymbol{\sigma}_M \cdot \boldsymbol{n}_M^+, \\ \boldsymbol{\lambda}_F - p_F \mathbf{I} \cdot \boldsymbol{n}_M^+ &= -\boldsymbol{\sigma}_M \cdot \boldsymbol{n}_M^-. \end{aligned} \tag{9}$$

Here, $\boldsymbol{\sigma}_M$ denotes the matrix thermo-poroelastic stress tensor, and $\boldsymbol{n}_M^\pm$ are the matrix outward normal vectors on each side of the fracture. The two sides of the fracture are denoted by "+" and "-", respectively. The normal to the fracture is chosen to be equal to the matrix normal on the (+) side. Consequently, the primary variables in the fracture are the temperature T, the pressure p, the displacement $\mathbf{u}$ and the contact traction $\boldsymbol{\lambda}_F$.

The fracture aperture of a dimensionally reduced fracture will be affected by fluid pressure as well as thermo-poromechanical forces in the matrix. It is given by

$$a = a_0 + [\![\mathbf{u}]\!]_\mathrm{n}, \tag{10}$$

with a_0 denoting the residual hydraulic aperture in the undeformed state, and $[\![\mathbf{u}]\!]_\mathrm{n}$ the normal component of a displacement-jump over the fracture, defined as

$$[\![\mathbf{u}]\!] = \mathbf{u}^+ - \mathbf{u}^-, \tag{11}$$

i.e., the difference in the displacement computed on the fracture walls on each side of the fracture (Figure 1b). A vector $\mathbf{b}_F$ can be decomposed into $b_n = \boldsymbol{b_F} \cdot \boldsymbol{n}_M^+$ and $\mathbf{b}_\tau = \boldsymbol{b_F} - b_n \boldsymbol{n}_M^+$, that is the normal and tangential components relative to the fracture.

The dilation of the fracture associated with a tangential (sharing) displacement $[\![\mathbf{u}]\!]_\tau$ due to the rough fracture surfaces is defined by a gap function (Stefansson, et al., 2021a):

$$g = \tan(\Psi)\, ||[\![\mathbf{u}]\!]_\tau||, \tag{12}$$

with Ψ as the dilation angle described by (Barton, 1976). Hence, g, is the normal distance between the fracture walls when in mechanical contact. The relative motion between the fracture walls is described by a nonpenetration condition which constrains the fracture deformation in the normal direction:

$$\begin{gathered} [\![\mathbf{u}]\!]_\mathrm{n} - g \geq 0, \\ \lambda_n([\![\mathbf{u}]\!]_\mathrm{n} - g) = 0, \\ \lambda_n \leq 0. \end{gathered} \tag{13}$$

It follows that the normal contact force, λ_n, is zero when a fracture is mechanically open and there is no mechanical contact across the fracture. Finally, a Coulomb friction law that governs sliding of the fracture is given:

$$\begin{gathered} ||\boldsymbol{\lambda}_\tau|| \leq -F\lambda_n, \\ ||\boldsymbol{\lambda}_\tau|| < -F\,\lambda_n \rightarrow [\![\dot{\mathbf{u}}]\!]_\tau = \mathbf{0}, \\ ||\boldsymbol{\lambda}_\tau|| = -F\,\lambda_n \rightarrow \exists\, \zeta \in \mathbb{R}^+ : [\![\dot{\mathbf{u}}]\!]_\tau = \zeta\boldsymbol{\lambda}_\tau. \end{gathered} \tag{14}$$

With, $\boldsymbol{\lambda}_\tau$, and $[\![\dot{\mathbf{u}}]\!]_\tau$ respectively, denoting the tangential contact force and displacement increment, and F denoting the friction coefficient.

The the Darcy velocity in the fracture is given by

$$\mathbf{v}_F = -\frac{k_F}{\eta}\left(\nabla_\parallel p_F - \rho_{f,F}\mathbf{g}_\parallel\right), \tag{15}$$

where the permeability in the fracture, k_F, is related to the aperture by the cubic law by $k_F = a^2/12$. Here, $\nabla_\parallel p_F$ denotes the pressure gradient and $\boldsymbol{g}_\parallel$ the component of the gravity vector, both in the plane of the fracture. The subscript F refers to quantities specific to the fracture. The cubic law gives a strongly non-linear relation between fracture aperture and fluid flow in the fracture. The mass balance equation for the fracture becomes

$$a\left(\frac{1}{B_f}\frac{\partial p_F}{\partial \mathrm{t}} - \beta_f\frac{\partial T_F}{\partial \mathrm{t}}\right) + \frac{\partial a}{\partial \mathrm{t}} + \nabla_\parallel \cdot (a\mathbf{v}_F) - v^+ - v^- = a\mathrm{Q}_{\mathrm{p,F}}, \tag{16}$$

where v^+ and v^- are volumetric fluxes into the fracture on each side of the fracture (Figure 1b). The energy balance equation for the fracture is

$$\begin{aligned} \rho_{f,F} c_f T_F \frac{\partial a}{\partial \mathrm{t}} + c_f a \frac{\partial\left(\rho_{f,F} T_F\right)}{\partial \mathrm{t}} + \nabla_\parallel \cdot \left[a\left(\rho_{f,F} c_f T_F \mathbf{v}_F - \kappa_f \nabla T_F\right)\right] - w^\pm - q^\pm \\ = a\mathrm{Q}_{\mathrm{T,F}}, \end{aligned} \tag{17}$$

where κ_f is the heat conductivity of the fluid and $w^\pm$ and $q^\pm$ are advective and conductive heat interface fluxes into to the fracture on each side.

The interface fluxes describe the flow of mass and energy between the fracture and rock matrix and are given with the following equations (Martin et al., 2005; Jaffré et al., 2011; Stefansson et al., 2021b):

$$v^\pm = -\frac{k_F}{\eta}\left(\frac{2}{a}\left(p_F - p_M^\pm\right) - \rho_{f,F}\mathbf{g}\cdot\mathbf{n}_{\boldsymbol{M}}^\pm\right), \tag{18}$$

$$q^\pm = -\frac{2\kappa_f}{a}\left(T_F - T_M^\pm\right), \tag{19}$$

$$w^\pm = \begin{cases} v^\pm \rho_{f,M}^\pm c_f T_M^\pm & \text{if } v^\pm > 0 \\ v^\pm \rho_{f,F} c_f T_F & \text{if } v^\pm \leq 0 \end{cases}. \tag{20}$$

Where the subscript F and M refers to properties in the fracture and matrix respectively, and the superscript $\pm$ refers to which side of the fracture those properties are taken. On the matrix boundary, the internal boundary conditions,

$$\mathbf{u}_M^\pm = \mathbf{u}^\pm, \quad \mathbf{v}_M^\pm \cdot \mathbf{n}_{\boldsymbol{M}}^\pm = v^\pm, \quad \mathbf{q}_M^\pm \cdot \mathbf{n}_M^\pm = q^\pm \quad \text{and} \quad \mathbf{w}_M^\pm \cdot \mathbf{n}_M^\pm = w^\pm, \tag{21}$$

ensure coupling from the variables in the matrix to the variables on the fracture wall. Here, $\mathbf{w}_M = \rho_{f,M} c_f T\mathbf{v}$ and $\mathbf{q}_M = -\kappa_\mathrm{e}\nabla T$ respectively defines the advective and conductive heat flux in the matrix. On the fracture tips zero Neumann conditions are imposed for the mass and energy balance.

Tensile stress and fracture propagation

The base for our numerical study is the conceptual model for CDM described in Axelsson (1985). It assumes that reservoir fluid circulates at the bottom of a permeable hydrothermal reservoir, with the circulation extending through fractures into a less permeable layer below. The circulating fluid cools down the rock surrounding a single fracture (Figure 1a), creating tensile stresses and causing the rock to contract and the fracture to open and propagate—given that the tensile force is sufficient to overcome other forces holding the fracture closed.

Following Stefansson et al. (2021b) we consider propagation due to tensile forces, modeled by the stress intensity factor, SI_{I}, given as a function of the normal component of the displacement-jump over the fracture:

$$SI_{\mathrm{I}} = \sqrt{\frac{2\pi}{R_d}}\Big(\frac{\mu}{\kappa + 1}[\![\mathbf{u}]\!]_{\mathrm{n}}\Big). \tag{22}$$

Where, R_d is the distance between the point where the displacement jump is evaluated and the fracture tip, and the Kolosov constant for plain strain is given by

$$\kappa = \frac{B_S + 7\mu/3}{B_S + \mu/3}. \tag{23}$$

For details, see for instance Nejati et al. (2015). Furthermore, introducing a propagation criterion (Stefansson et al. (2021b), with the fracture tip propagating when SI_{I} exceeds a critical value:

$$SI_{\mathrm{I}} \geq SI_{Icrit}. \tag{24}$$

The critical value can be viewed as the rock toughness or the resistance of the rock to fracture.

Notes on the numerical implementation

The mathematical model for the thermo-poroelastic fractured medium with fracture mechanics and matrix-fracture mass and energy fluxes, is implemented in the open-source simulation tool PorePy, which is tailored for representing complex multiphysics processes in fractured porous media, see Keilegavlen et al. (2021a) for more information. The fractures are explicitly represented in the computational grid which allows for detailed modelling and provides high resolution of processes in the fracture and on the fracture-matrix interface (fracture walls). Moreover, fracture propagation is represented by extending the fracture grid, with minimal adjustments needed to the rest of the computational model.

In the computational grid, pressure and temperature are represented in both rock matrix and fracture, while the displacement is confined to the rock matrix and on the fracture walls and contact tractions are represented on the fractures (Figure 1b). The full set of degrees of freedom and their coupling structure is described in Stefansson, et al. (2021b), where implementation details including the algorithm for fracture propagation can also be found. In accordance with the conceptual model, we make the simplifying assumption that the propagation will be tensile and in the vertical direction. Therefore, the grid is aligned in the vertical direction, with the pre-existing fractures conforming to the grid, and the propagation is restricted to follow grid cell edges.

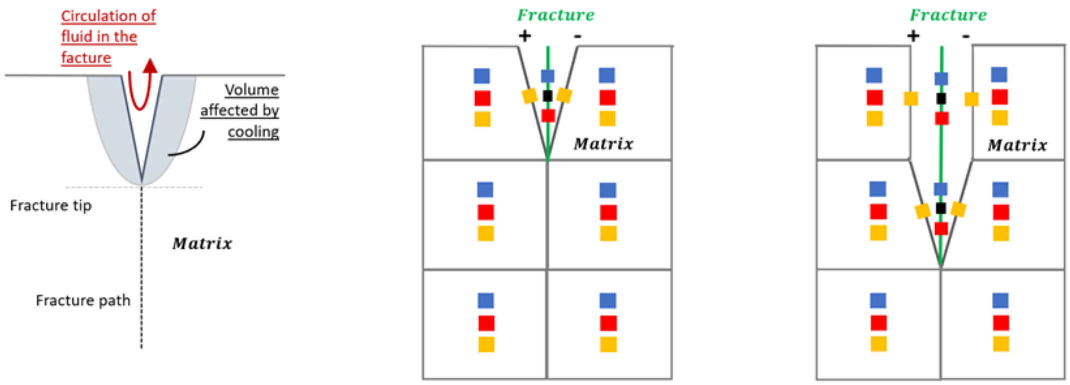

Figure S1. a) Conceptual model for CDM in a single open fracture, adapted from Axelsson (1985). b) Schematic of the mixed-dimensional computational grid: Pressure and temperature (blue and red) are modelled in both the rock matrix and the fracture, while the displacement (yellow) is computed in the rock matrix and on the opposing fracture walls ("+" and "-" side of the fracture). In the fracture contact traction force is shown (black) but not shown are the interface fluxes on the fracture walls, describing the flow of mass and energy between the fracture and rock matrix. c) Same schematic as b) but after the fracture has propagated one vertical grid-block downward. In the mathematical model and on the computational grid, there is no separation between the fracture and the fracture walls, still this is shown on b) and c) for visualization purposes.